Available online at www.sciencedirect.com
SCIENCE DIRECT®
Journal of Nuclear Materials 326 (2004) 132–143
journal of nuclear materials
www.elsevier.com/locate/jnucmat

A study of molybdenum behaviour in UO_2 by X-ray absorption spectroscopy

Philippe Martin [a,*], Michel Ripert [a], Gaëlle Carlot [a], Philippe Parent [b], Carine Laffon [b]

[a] CEA-Cadarache, DEN/DEC/SESC/LLCC, Bâtiment 151, 13108 Saint-Paul lez Durance cedex, France
[b] LURE, Université Paris-Sud, Bâtiment 209D, 91405 Orsay cedex, France

Received 20 March 2003; accepted 6 January 2004

Abstract

Molybdenum is one of the most abundant fission products created in UO_2 fuel. Post-irradiation examinations show that molybdenum is mainly associated with rhodium, ruthenium, palladium and technetium in metallic precipitates. However, for low burn-ups, these five metal particles cannot be detected. In order to determine the chemical state of molybdenum in UO_2, XANES experiments were carried out on fresh UO_2 pellets implanted with Mo ions. The measurements performed at the oxygen K and molybdenum L_{III} edges showed a correlation between the chemical state of molybdenum and the O/U ratio of the UO_2 matrix. Indeed, the molybdenum located at the grain boundaries is present in both metallic and +IV oxidation states. To our knowledge, this study is the first experimental evidence of the solution annealing of Mo^{+IV} in the cationic lattice of UO_2. Thus, when molybdenum is oxidised at the +IV state, it remains in solution in the UO_2 matrix.

PACS: 61.10.Ht; 64.75.+g; 28.41.Bm

1. Introduction

Among all the fission products, molybdenum has a very significant role in the chemistry of nuclear fuel. Moreover, this element is one of the most abundant fission products because of its fission yield which is equivalent to that of xenon [1]. This abundance would in itself justify a detailed study of its behaviour. But what makes molybdenum particularly relevant is that the oxygen potential of the Mo/MoO_2 couple is situated very close to that of the stoichiometric UO_2 [1]. Being a buffer in uranium dioxide oxidation [1–3], molybdenum therefore has a major influence on UO_2 oxygen potential. The chemical state of molybdenum should thus be a sensitive indicator of the fuel oxidation state. Usually, in irradiated fuel, a partitioning between oxide and metal phases is observed [2].

Out of reactor, the noble metals form separate metallic precipitates containing the five elements, Mo, Tc, Ru, Rh and Pd. Electronic microscopy studies [4] showed that the metal particles were located both within grain boundaries and inside UO_2 grains. These particles usually exhibit the ε-Ru (Mo, Tc, Rh, Pd) phase structure. But, for low burn-up samples, the five metal particles were not detected by electron microprobe analysis (EMA). This result cannot exclude that molybdenum forms nanometric metallic clusters which, due to resolution, cannot be observed by EMA.

Thermal diffusion studies showed that Mo exhibits effective diffusion coefficients significantly lower than those of elemental species such as Xe or I in the 2023–2098 K temperature range [5]. However, the molybdenum release rate is not nil, as opposed to soluble fission

* Corresponding author. Tel.: +33-4 42 25 38 66; fax: +33-4 42 25 37 13.
E-mail address: martinp@drncad.cea.fr (P. Martin).

0022-3115/$ - see front matter © 2004 Elsevier B.V. All rights reserved.
doi:10.1016/j.jnucmat.2004.01.006

products such as zirconium. This is confirmed by Kleykamp's results [6] which highlighted that the maximum solubility of molybdenum in UO_2 is lower than 0.006 mol%.

It is thus possible that for kinetic reasons a fraction of molybdenum remains in the UO_2 matrix and could be associated with a Schottky type defect. This is a very important point, because if Mo has not precipitated and is in a state close to the one it would have been in if it had been oxidised, its impact on swelling would be increased by 0.15%/10 GWj/t [7]. In order to determine the influence of molybdenum on the swelling of UO_2 pellets, it would be enough to know its chemical state (oxidation rate) as a function of burn-up, particularly at low burn-up.

Classically, the X-ray Absorption Spectroscopy (XAS) allows the probing of both the oxidation state and the atomic local environment of the absorbing atom. To our knowledge, very few XAS studies have been performed on nuclear fuels [8,9]. This technique, and particularly the X-ray Absorption Near Edge Structure (XANES) spectroscopy at the Mo L_{III} edge ($E_0 = 2520$ eV), will thus be applied here. Indeed, with this technique, it is possible to probe the 4d valence orbitals of molybdenum involved in the chemical bonds which are particularly sensitive to local symmetry [10]. It should be noted that a study at the K edge is impossible because the fluorescence lines of molybdenum are located at the same energy as those of uranium.

Therefore, this study focuses on the evolution of molybdenum implanted in UO_2 pellets before and after thermal annealing. First, the surface of the fresh UO_2 samples will be characterised by X-ray absorption spectroscopy at the oxygen K edge ($E_0 = 543.1$ eV). At this low energy, it is possible to probe the extreme surface of the sample (<0.1 μm). The data analysis will show if the samples' surface oxidises during the different handling steps between the facilities for thermal treatment (Cadarache, France) and those for measurements (Orsay, France). Second, as a function of annealing conditions, the evolution of the molybdenum L_{III} edge spectra obtained in both fluorescence and Total Electron Yield (TEY) detection mode will be studied. The comparison between the spectra obtained with these two detection modes on the same sample will help discriminate the answer of Mo ions located at the surface.

2. Experimental details

2.1. Sample preparation

All the measurements were carried out on depleted (0.3% of uranium 235) UO_2 discs of 8.2 mm in diameter and 1 mm thick. All the samples were polished down to 1 μm with diamond paste. Before implantation, the samples were annealed at 1273 K during 8 h under reducing atmosphere (Ar + 5% H_2) in order to relax the structural stresses due to the polishing process and to reach stoichiometric $UO_{2.00}$.

The UO_2 pellets were implanted with 400 keV $^{98}Mo^+$ ions at the *Institut de Physique Nucléaire de Lyon* (IPNL). For this energy, the mean range estimated with the SRIM2000 code [11] is about 90 nm. The nominal dose was 1.6×10^{16} ions cm^{-2} corresponding to a mean Mo concentration of 1.0 at.% on the first 150 nm of the target. The beam current during implantation was typically 10 μA cm^{-2}. Each sample then underwent a reducing annealing (Ar + 5% H_2) at 1273 K between 4 and 48 h.

2.2. X-ray absorption near edge structure (XANES)

2.2.1. Oxygen K edge

The oxygen K edge ($E_0 = 543.1$ eV) XANES was performed at room temperature in fluorescence detection mode on the SA22 beamline of the LURE SUPERACO storage ring (*Laboratoire pour l'Utilisation du Rayonnement Electromagnétique*, Orsay, France), which operated at an energy of 800 MeV with a current of 215–407 mA. Because of the very low energy of this edge, all the measurements were carried out with an ultra-high vacuum device ($P \sim 10^{-9}$ Torr). The energy scale was calibrated by setting the position of the first peak of Cr_2O_3 at 532.0 eV. The resolution of the experimental device is estimated at 0.2 eV [12]. The intensity of each XANES spectrum is normalised after the main resonance of the edge structure using the 541.0 eV position. The residual background noise is eliminated by subtracting a linear function in the pre-edge zone. In order to be consistent with the value given in the literature [13,14], a constant shift of −2.0 eV had to be applied to our data. After this correction, the energy positions of the various resonances were determined with the second derivative spectra.

2.2.2. Molybdenum L_{III} edge

The Mo L_{III} edge ($E_0 = 2520.0$ eV) XANES spectra were recorded on the SA32 beamline of the LURE SUPERACO storage ring. A Ge(1 1 1) double crystal monochromator was used. After each sample, the energy was calibrated at the sulphur K edge ($E_0 = 2473.0$ eV) using the ZnS compound as a reference, leading to an energy resolution of about 0.3 eV. In order to be able to discriminate the information related to the surface of samples from that coming from the bulk, two types of detection were used:

- the TEY mode which allows the Mo atoms to be probed on the first 30 nm of the sample,
- fluorescence detection with an analysis depth of about 1 μm which provides information on all the Mo ions implanted in the targets.

The intensity of each XANES spectrum is normalised versus to the 2532.0 eV position located after the white line. The pre-edge background is subtracted by fitting a linear function in the pre-edge region.

The origin of Mo L_{III} edge XANES is mainly the electron transition from a core level ($2p_{3/2}$) to a vacant 4d state. Thus, as the local symmetry around Mo atoms evolves, different splittings of the white line, due to the local crystal field, will be observed. In order to interpret such a feature, a deconvolution model is applied to the experimental data. This means applying an arctangent function to describe the absorption jump, and a sum of Gaussian functions to take into account the different 4d states. This deconvolution process was performed using a least squares fitting procedure to reproduce the normalised spectra with the expression:

$$F(E) = \frac{1}{2} + \frac{1}{\pi} \times \arctan\left(\frac{2 \times (E - E_0)}{\tau}\right) + \sum_i \frac{A_i}{\omega_i} \times \sqrt{\frac{4 \times \ln(2)}{\pi}} \times \exp\left(\frac{-4 \times \ln(2) \times (E - E_{0_i})^2}{\omega_i^2}\right),$$

where E is the photon energy (eV), E_0 the edge energy (eV), τ the core hole lifetime (1.78 eV for Mo L_{III} edge), A_i the intensity of the i transition, ω_i the width of the i transition (eV) and E_{0i} the peak position (eV).

The results will be compared to the values obtained for different reference compounds in order to estimate the oxidation state as well as the local symmetry around molybdenum.

3. Results

First, the spectra collected at the oxygen K edge will be explained. Their interpretation will allow us to see if the sample surface is still stoichiometric $UO_{2.00}$. In the second part, the measurements performed at the molybdenum L_{III} edge are presented for:

- Some molybdenum compounds whose crystallographic structure is well known. The interpretation of these spectra will help us to analyze data obtained for UO_2 pellets.
- The pellets implanted with molybdenum before and after heat treatment.

3.1. Fresh UO_2

An X-ray absorption spectrum at the oxygen K edge corresponds to an electric dipole transition O 1s → O *n*p, $n \geqslant 2$. In the case of oxide edges, the absorption structures observed on the domain (E_0, $E_0 + 10$ eV) mainly come from the excitation channel O 1s → O 2p [15]. This zone thus gives a picture of the electronic structure of the empty states of the oxygen atoms. In the case of UO_2, ab initio calculations based on the linear muffin-tin orbital (LMTO) method in the LSDA + U approximation give excellent results [13].

The space group of uranium dioxides is $Fm\bar{3}m$ with a cell parameter $a = 5.470$ Å. The atomic co-ordinates in the unit cell are uranium at $(0, 0, 0)$ and oxygen at $(0.25, 0.25, 0.25)$. In the XANES spectra, the zone at higher energy ($>E_0 + 10$ eV) corresponds to the multiple scattering processes on the atoms of the matrix [16]. The positions of the various peaks in this zone give the crystalline symmetry around the oxygen atoms. In the UO_2 spectrum, five resonances are observed [14].

The oxygen K edge spectrum of a UO_2 single crystal is shown in Fig. 1. The four main features directly connected to the electronic structure are labelled a, b, c and d while the ones related to the crystallographic structure are referenced A, B, C, D and E. Their energy positions compared to those of Ref. [13] are gathered in Table 1. The data are in full agreement, confirming the stoichiometry $UO_{2.00}$ for the single crystal.

The XANES spectra of a single crystal and a fresh fuel pellet are compared in Fig. 2. The main features of the multiple scattering process, characteristic of the face-centred cubic structure of UO_2 are still observed, even if some little shifts have occurred. This observation shows that the crystallographic symmetry is maintained. However, a clear difference in the electronic structure can be noted with in particular, the existence of an intense peak at low energy. This result seems to indicate a probable oxidation of the sample surface.

During the same experiment, the spectrum of the α-U_3O_8 compound (compound obtained at the end of the oxidation of UO_2 [17] in air) was collected. In order

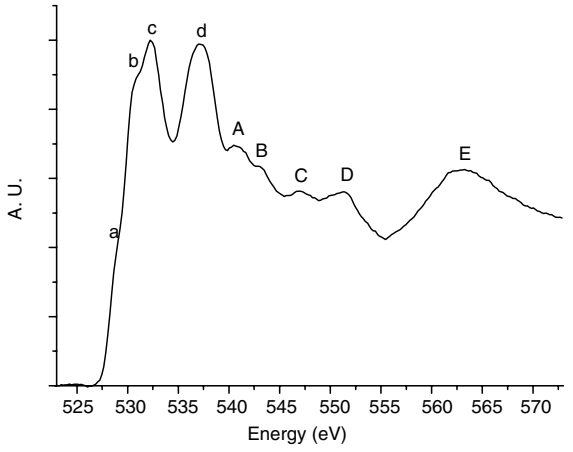

Fig. 1. XANES spectra at oxygen K edge of a UO_2 single crystal.

Table 1
Energies of the resonance of the O K edge spectra

Compound	a	b	c	d	A	B	C	D	E
UO_2 [13]	528.55	530.65	532.2	537.0	540.9	543.1	546.85	551.85	564.05
Single crystal	528.6	530.4	532.2	537.0	541.0	543.1	546.8	551.5	563.9
UO_2 pellet	529.2		532.6	536.1	541.4	543.6	546.9		563.7

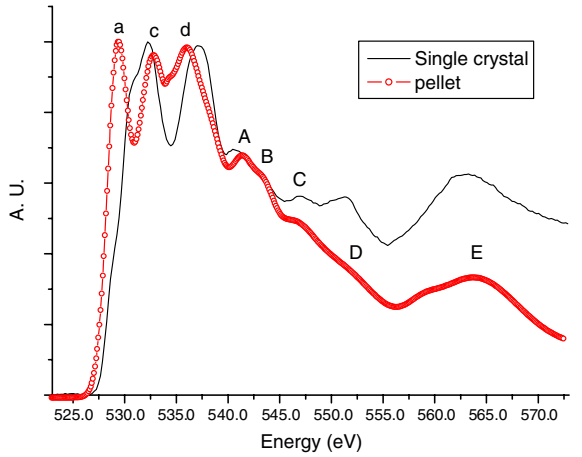

Fig. 2. XANES spectra obtained at oxygen K edge for a single crystal and a fresh UO_2 pellet.

to determine the presence of this compound on the surface of our samples, an attempt was made to reproduce our experimental spectrum by a linear combination of UO_2 and α-U_3O_8. The impossibility seems to exclude the presence of this last phase, both at the surface and in the bulk of the sample.

To interpret the differences observed in Fig. 2, electronic structure calculations were performed by F. Jollet, using the LMTO method in the LSDA + U approximation (method detailed in Ref. [13]). The results are presented in Fig. 3, where the total densities of states (DOS) are shown, as projected on the oxygen 2p orbital, obtained for UO_2 and a UO_2 supercell, made of two normal cells, with an additional oxygen atom positioned in the octahedral site of the fluorite structure $(1/2, 1/2, 1/2)$. It is important to note that this calculation was only made to see if the presence of an additional oxygen atom modified the total electronic structure of the oxygen atoms. The crystallographic position used here can appear to be in contradiction with the positions of the oxygen interstitials described by Willis et al. [18–20] in UO_{2+x}. But, for this compound, the presence of interstitials is systematically linked to the

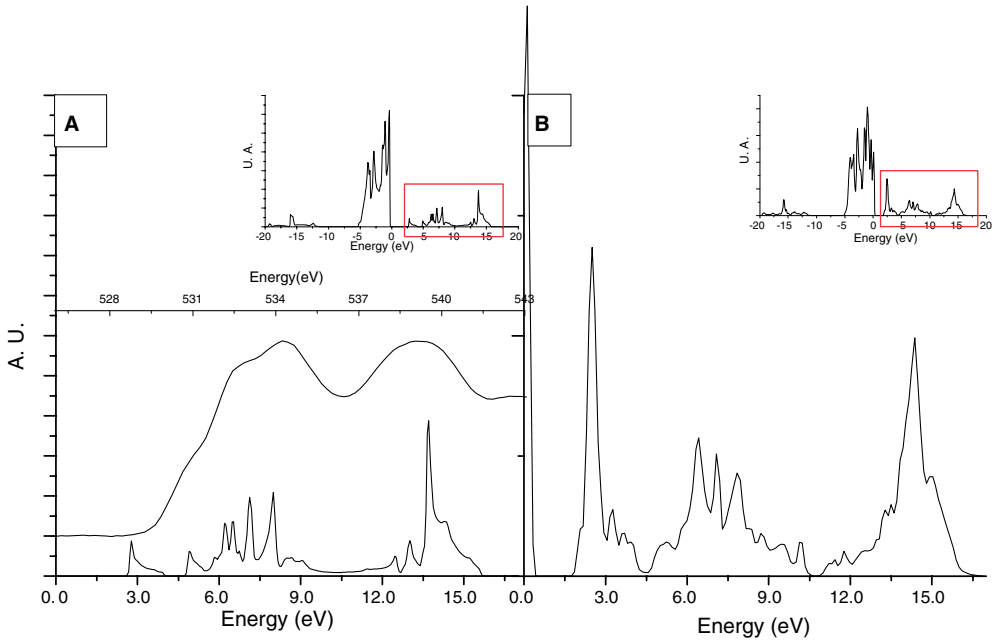

Fig. 3. Oxygen 2p calculated projected density of state in the frame of an LSDA + U approach: $UO_{2.00}$ cell (A); UO_2 + interstitial supercell (B). The zero of energy is the Fermi level.

presence of oxygen and uranium vacancies, thus forming complex defects and implying the use of more than two elementary cells to be modelled. This cannot be done with the code used here. An average position representative of the oxygen defects in hyper-stoichiometric uranium dioxide was used in order to highlight a general tendency.

Because only the empty states are probed by XAS, a zoom is realised on the latter. As shown by Jollet et al. [13,14], the DOS projected on the oxygen 2p orbital reproduced the O K edge of $UO_{2.00}$. The comparison of the two calculated DOS shows that in the supercell case, an intense empty state appears at low energy, approximately 2.9 eV above the Fermi level. The presence of oxygen atoms in interstitial positions should reveal an intense peak at low energy in our spectra.

In accordance with the calculations described above, an intense resonance at low energy (531.2 eV) is actually observed in our spectrum, indicating the presence, in a regular way, of oxygen atoms in the octahedral sites of the face-centred cubic structure. This result is described as the first stage of the $UO_{2.00}$ oxidation in the formation of an intermediary phase of a hyper-stoichiometric oxide such as U_4O_9 [21] via complex cuboctahedral defects as described by Nowicki et al. [22]. The structural model proposed by those authors implies, as in this study, the preservation of the face-centred cubic symmetry.

With this result, it is shown that even if the air exposure of our samples is slight, their surface is slightly hyper-stoichiometric, while keeping an O/M ratio lower than 2.25 (equivalent to U_4O_9). Thus, the fact that the surface of our samples will be systematically oxidised must be taken into account in the analysis of spectra.

3.2. Reference compounds

As described in the introduction, molybdenum is almost insoluble in UO_2. It is thus expected to be found in metallic and/or oxide separated phases. To be able to identify this form, the XANES spectra of various reference compounds were recorded in TEY mode. These compounds have been selected in order to distinguish both molybdenum oxidation state (0, +IV or +VI) and local symmetry (tetrahedral or octahedral) in our experimental spectra. The two most common oxides MoO_2 and MoO_3 which are expected to be present in our samples are presented. They are compared with compounds where molybdenum is at same oxidation state but with different local symmetry in order to determine if such feature has an impact on white line position. They are all presented in Fig. 4 where they are shifted upwards for improved clarity. The local environments and oxidation states of molybdenum in these compounds are the following:

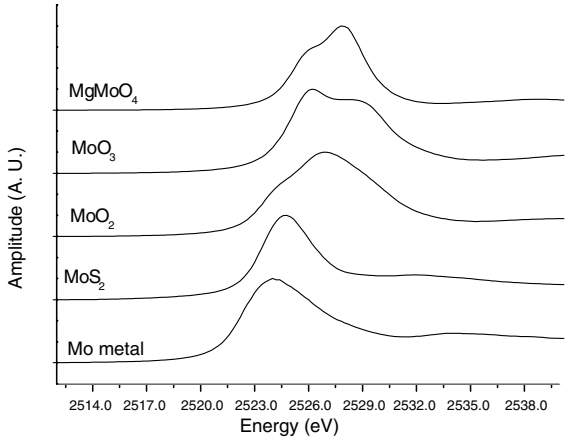

Fig. 4. Mo L_{III} edge XANES spectra of reference compounds obtained in total electron yield.

- MoO_3 (Mo^{+VI}): crystallises in the orthorhombic system and belongs to the Pbnm space group ($a = 3.9628$ Å, $b = 13.855$ Å and $c = 3.6964$ Å) [23]. In this structure, molybdenum is surrounded by six oxygen atoms forming a distorted octahedron with the following distances: Mo–O(1) = 1.67 Å, Mo–O(2) = 1.73 Å, 2 × Mo–O(3) = 1.95 Å, Mo–O(2) = 2.25 Å, Mo–O(3) = 2.33 Å. MoO_3 is made of a stacking of layers containing two parallel layers of octahedrons MoO_6.
- $MgMoO_4$ (Mo^{+VI}): in this compound, molybdenum is surrounded by four oxygen atoms, forming a regular tetrahedron.
- MoO_2 (Mo^{+IV}): crystallises in the monoclinic system and belongs to the $P2_{1/C}$ space group ($a = 5.6109$ Å, $b = 4.8562$ Å, $c = 5.6285$ Å and $\alpha = 120°57$) [24]. In this structure, molybdenum atoms are surrounded by six oxygen atoms forming a distorted octahedron with the following distances: Mo–O(1) = 1.942 Å, 2 × Mo–O(1) = 1.982 Å, Mo–O(2) = 1.995 Å, Mo–O(2) = 2.059 Å, Mo–O(2) = 2.071 Å. MoO_2 can be described as chains of MoO_6 octahedrons bounded by corners and edges.
- MoS_2 (Mo^{+IV}): in this compound, molybdenum is surrounded by six sulphur atoms forming a very distorted octahedron. The characteristic of this compound is that, contrarily to the oxides described here, no splitting of the white line into two components is observed [10].
- Metallic Mo: has a centred cubic structure with a cell parameter of 3.147 Å.

The second derivatives of these spectra, presented in Fig. 5, highlight a splitting of the white line into two components in the case of MoO_2, MoO_3 and $MgMoO_4$. This feature is attributed to the 4d splitting due to the crystal field created by the oxygen atoms surrounding

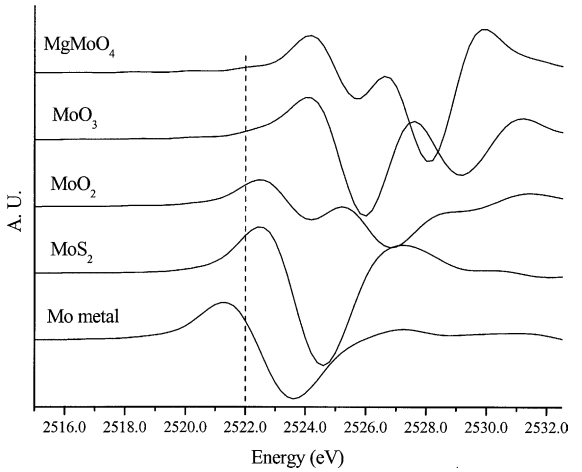

Fig. 5. Second derivatives of Mo L_{III} edge XANES spectra of reference compounds obtained in total electron yield. The dashed line represents the metal E_0 position.

the molybdenum ions. In the case of the octahedral symmetry observed in MoO_2 and MoO_3, one can speak about the orbital t_{2g} and e_g^*, while in the case of tetrahedral symmetry, as in $MgMoO_4$, one can speak about the orbital e_g and t_2^* [25]. The relative intensity of the two components of the white lines is a function of the transition probability ($t_{2g}/e_g^* = 2/3$ and $e_g/t_2^* = 3/2$). This feature is fully described in Ref. [10].

The numerical values are gathered in Table 2. The first observation lies in the correlation between the oxidation state and the edge position: 2522.0 ± 0.2 eV for Mo^0, 2523.5 ± 0.2 eV for Mo^{+IV} and 2525.0 ± 0.2 eV for Mo^{+VI}. Moreover, it appears that for a tetrahedral symmetry, the splitting of the two components is equal to 2.3 ± 0.2 eV, while for an octahedral symmetry, this value varies with the oxidation state: 3.2 eV for Mo^{+VI} and 2.6 eV for Mo^{+IV}. Generally, the splitting between the two peaks is always shorter for a tetrahedral symmetry [26].

Furthermore, Aritani et al. [25], who obtained the same values, showed that the reduction of molybdenum from +VI to +IV, causes a shrinking of the energy levels. However, as it also implies a lowering of the edge, the difference between a reduction and a modification of symmetry can be made. Moreover, the same authors, in a study of Mo^{+VI} organic compounds with a distorted octahedral symmetry of $P_2O_5 \cdot 24MoO_3 \times H_2O$ and $(NH_4)_6Mo_7O_{24} \times H_2O$, highlighted that the weakening of Mo–O bonds, because of the distortion of the local environment, causes a reduction of the shifts between levels t_{2g} and e_g^*. In this case, the differences between the two components of the white line range from 2.8 to 2.9 eV with a position of the first component identical to that of MoO_3 (2526.0 eV).

With the values thus obtained, we will be able to determine both the molybdenum oxidation state and the local symmetry as a function of the gap between white line components.

First of all, we analyzed the as implanted samples.

3.3. As implanted samples

As we can see in Fig. 6, the spectra obtained in TEY and fluorescence modes are very different. The fit results and second derivative spectra are presented in Fig. 7. From these last spectra, the number of Gaussian components needed to reproduce the fine structure of the white line were determined. The numerical values obtained are given in Tables 3 and 4 for TEY and fluorescence detection respectively.

In the TEY case, the edge energy is equal to 2524.4 eV, indicating an oxidation state ranging from +IV to +VI. In order to simulate this spectrum, only two Gaussian components centred at 2525.9 and 2529.0 were necessary, resulting in an energy gap of 3.1 eV. These values are very close to those measured for MoO_3. This would seem to indicate that the molybdenum located on the surface has precipitated into MoO_3 (the most stable molybdenum oxide at ambient temperature), which is in contradiction with the edge energy. So, in addition to MoO_3, a part of the molybdenum ions is present in an oxidation state lower than +VI.

In the fluorescence case, the value of E_0 is equal to 2523.0 eV, indicating a mean oxidation state lower than +IV. It should be noted that, in this case, as opposed to the TEY one, all the molybdenum ions are probed. Three Gaussian functions centred at 2524.2; 2526.2 and 2529.0 eV had to be introduced to reproduce the experimental spectrum. The last component can be directly connected to the TEY measurement and is due to the presence of MoO_3. Its very low intensity is a good

Table 2
Edge position (E_0) and energy gap between the components of the white line obtained for reference compounds at Mo L_{III} edge

Compound	Oxidation state	E_0 (eV)	Local symmetry	Peak energy (eV)		ΔE (eV)
$MgMoO_4$	+6	2525.0	T_d	2525.7	2528.0	2.3
MoO_3	+6	2524.9	O_h (distorted)	2526.0	2529.2	3.2
MoO_2	+4	2523.5	O_h (distorted)	2524.1	2526.7	2.6
MoS_2	+4	2523.4	D_{3h}	2524.6		
Mo metal	0	2522		2523.6		

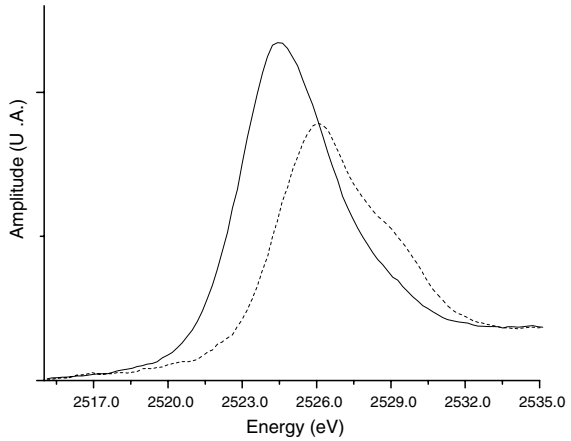

Fig. 6. As implanted XANES spectra of Mo L_{III} edge collected in TEY (- - -) and fluorescence (—) detection modes.

confirmation that MoO_3 precipitation is only located at the grain surface. The peak located at 2525.9 eV in the TEY mode is included in the 2526.2 eV component. The interpretation of the two first peaks is more complex. The first one is located at the same energy as for MoO_2 (2524.2 eV). However, the existence of this compound has to be excluded because on the one hand, the energy gap of 2.0 eV between the two components is too weak and, on the other hand, the ratio between the peak intensities has not been ascertained. The existence of these peaks would thus indicate the presence of Mo^{+IV} in a non-octahedral symmetry, and could correspond to a fraction of Mo ions dissolved inside the UO_2 structure.

In addition to these two oxidised forms, the fact that the edge energy (2523.0 eV) is lower than 2523.4 (pure Mo^{+IV}) could indicate that a part of the intragranular molybdenum is already in a metallic state.

3.4. Thermal study

3.4.1. Surface: total electron yield measurements

The spectra collected for the samples annealed during 4 and 8 h at 1273 K are presented in Fig. 8. The spectra corresponding to a longer annealing time cannot be recorded. In order to reproduce experimental data, three Gaussian components had to be considered in the fitting procedure. In Fig. 9, the fit obtained for 8 h of annealing is presented. Numerical values are gathered in Table 3.

It appears that the energy position E_0 varies inversely to the heat treatment duration. The shift from 2524.4 to 2523.5 eV indicates that the mean oxidation state decreases in the probed zone.

According to Ressler et al. [27], MoO_3 is reduced to Mo metal under a slightly reducing atmosphere, such as the one used in our study (Ar + 5% H_2). This reaction follows these successive stages:

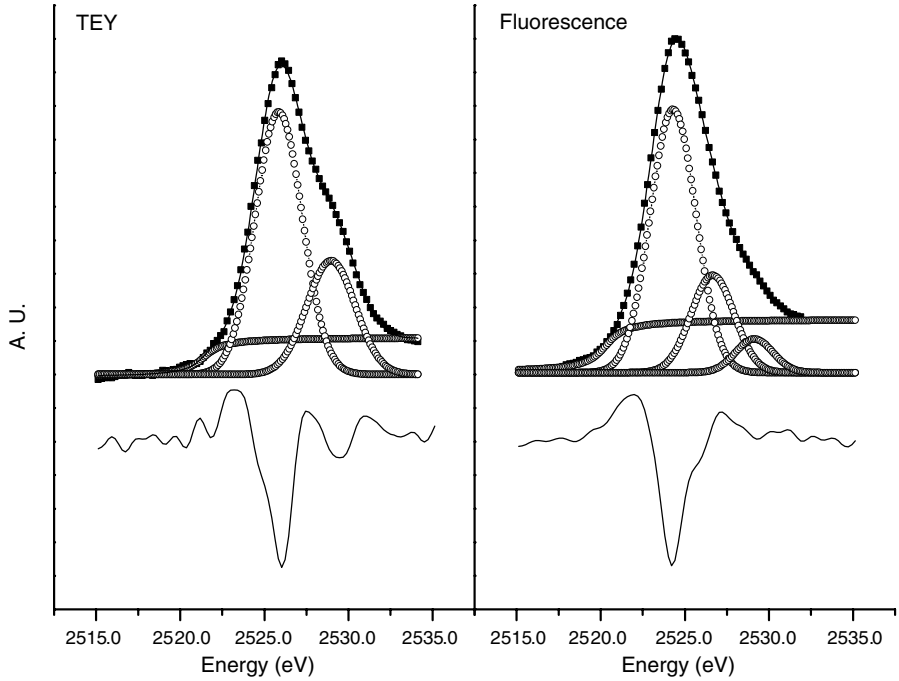

Fig. 7. Second derivative and best fit results at Mo L_{III} edge for as implanted sample obtained in TEY and fluorescence mode (experimental data (■), fit (—) and Gaussian functions (—○—)).

Table 3
Results obtained in TEY mode at Mo L_{III} edge

Annealing time (h)	Edge energy (eV)	Position (eV)	ΔE (eV)
0	2524.4	2525.9	3.1
		2529.0	
4	2524.1	2523.8	2.2
		2526.0	2.8
		2528.8	
8	2523.5	2523.8	2.2
		2526.0	2.8
		2528.8	

Table 4
Results obtained in fluorescence mode at Mo L_{III} edge

Annealing time (h)	Edge energy (eV)	Position (eV)	ΔE (eV)
0	2523.0	2524.2	2.0
		2526.2	2.8
		2529.0	
4	2522.9	2524.2	2.0
		2526.2	2.5
		2528.7	
8	2522.9	2524.0	1.9
		2525.9	2.5
		2528.4	
16	2522.8	2524.1	2.2
		2526.3	2.5
		2528.8	
24	2522.8	2523.6	2.0
		2525.6	2.6
		2528.2	
48	2522.6	2523.9	2.0
		2525.9	2.4
		2528.4	

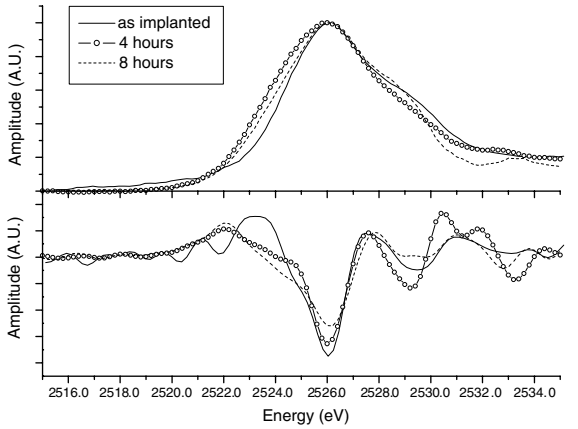

Fig. 8. Evolution of XANES and second derivative spectra at Mo L_{III} edge in TEY mode as a function of annealing time.

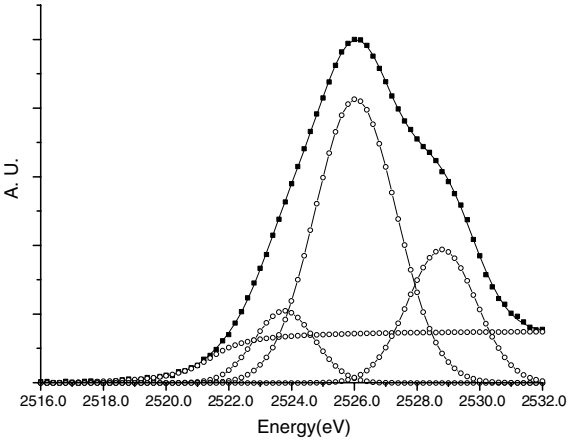

Fig. 9. Best fit result for 8 h annealing sample measured in TEY mode. Experimental data (■), fit (—) and Gaussian functions (—O—).

$$MoO_3 + H_2 \rightarrow MoO_2 + H_2O$$

$$3MoO_3 + MoO_2 \rightarrow Mo_4O_{11}$$

$$Mo_4O_{11} + 3H_2 \rightarrow 4MoO_2 + 3H_2O$$

$$MoO_2 + 2H_2 \rightarrow Mo + 2H_2O$$

These authors also indicate that for temperatures higher than 773 K, the oxide layer evolves into a pure Mo_4O_{11} phase. Two components located at 2528.8 and 2526.0 eV appeared in our measurements. This observation indicates an oxidation state of +VI and probably a distorted octahedral symmetry. This description is very similar to the one evidenced for the intermediate molybdenum oxides such as Mo_4O_{11} [28].

According to literature [29,30], when uranium dioxide is thermal treated in the presence of a molybdenum oxide at a temperature higher than 1073 K, a uranium molybdate precipitation is observed. The composition of the final product evolves between $UMoO_5$ and UMo_5O_{16}, according to the relative concentrations of the two starting oxides. In all these compounds, molybdenum has an oxidation state of +VI and is surrounded by six oxygen atoms forming a distorted octahedron with a distribution of the molybdenum–oxygen distances similar to the one given for MoO_3. Thus, if such a uranium molybdate appears, two components in the white line are expected. The first should be located at 2526.0 eV and the second at an energy gap of about 3 eV as described by Aritani et al. [25]. Consequently, it appears impossible to differentiate the formation of a

uranium molybdate with the presence of an intermediate molybdenum oxide. But considering our experimental conditions, the formation of uranium molybdate is not thermodynamically favourable. Thus, the presence of a Mo_4O_{11} intermediate oxide type seems to be the most probable solution.

Whatever the hypothesis considered, the result obtained for the sample as implanted clearly shows that the peak located at 2523.8 eV corresponds to a presence of Mo atoms in the matrix grains. This component is very similar to that observed for the molybdenum metal. Simultaneously, a decrease of the edge position E_0 to 2523.5 eV is observed. Thus the existence of Mo metal inside UO_2 grains appears to be the most likely scenario. The data collected in fluorescence mode will confirm this result.

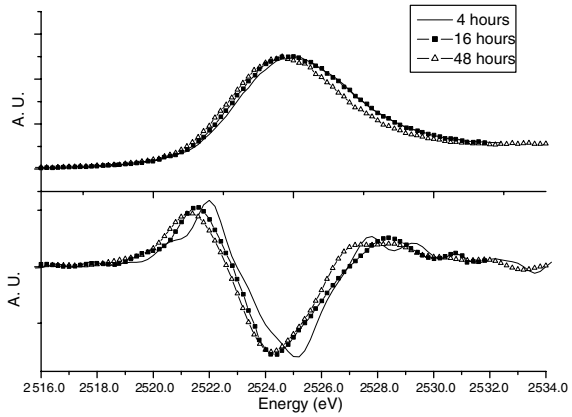

Fig. 10. Evolution of XANES and second derivative spectra at Mo L_{III} edge in fluorescence mode as a function of annealing time.

3.4.2. Fluorescence measurements

The signals collected in fluorescence detection mode are shown in Fig. 10 while the numerical values are given in Table 4. As for the as implanted samples, the white lines are made of three components whatever the annealing time. An example of fitting is given in Fig. 11. The first observation that can be made is that the inflexion point of the white line varies inversely to the annealing time. It clearly shows that the overall oxidation state of molybdenum in our samples decreases. Since the values given in Table 4 are systematically much lower than those observed for pure Mo^{+IV}, the presence of metallic molybdenum is the most probable assumption.

The general shape of the white line is almost the same for the different annealing times. The first two components located at approximately 2524.0 and 2526.0 eV, and thus at a distance of 2.0 eV, are the major components of these XANES spectra. The TEY measurements

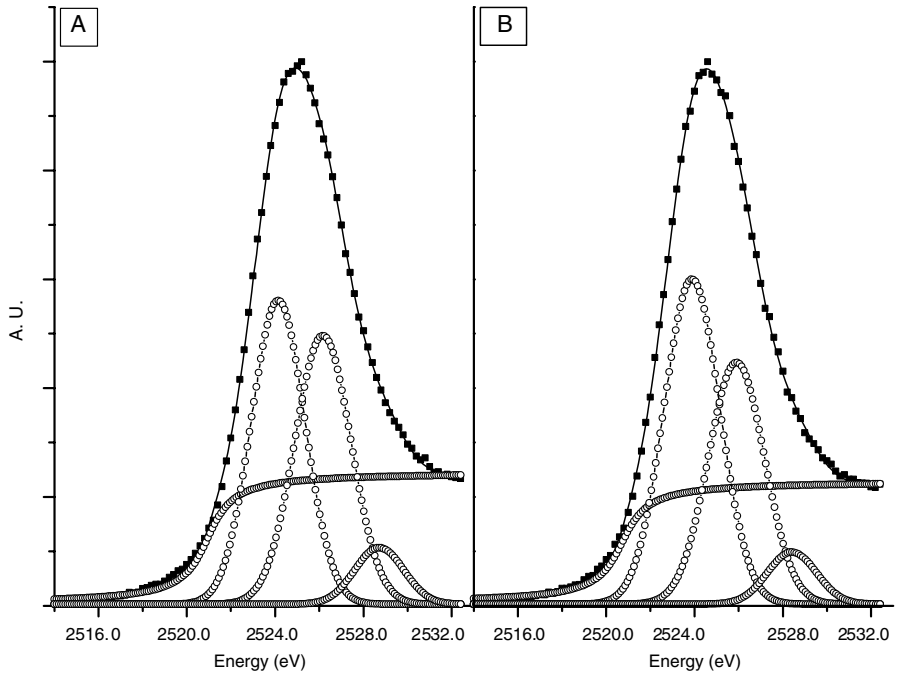

Fig. 11. Best fit result for 4 h (A) and 48 h (B) annealing samples measured in fluorescence mode. Experimental data (■), fit (—) and Gaussian functions (—O—).

with two peaks at 2528.8 and 2526.0 eV, helped to highlight the presence of a Mo^{+VI} compound at the surface and at the grain boundaries. The measurements in fluorescence mode clearly show the persistence of these two components. However, as for the as implanted sample, the significant amplitude difference between the two detection modes shows that the component located at 2526.0 eV clearly corresponds to another local environment of molybdenum. The first peak is located between the position of those found in the Mo reference foil and in Mo^{+IV}. The energy resolution does not allow us to consider two peaks in such a small interval. The components corresponding to metallic Mo and to Mo^{+IV} are thus included in this single peak. The most probable assumption is the presence of Mo^{+IV}, with a 2.0 eV separation of orbital lower than that of an octahedral environment.

The usual methodology used to determine the amounts of the different local environments of molybdenum, consists in reproducing the experimental data as a linear combination of the spectra of several reference compounds [10,26,31,32]. Initially, a simulation of our experimental spectra obtained in fluorescence mode by a linear combination of those of MoO_3 and metallic Mo was attempted. No result is given here because whatever the metallic molybdenum content, it was not possible to reproduce any of our experimental spectra. Moreover, the position of the maximum of the first Gaussian component in our XANES spectra does not correspond to that observed in metallic Mo. It thus appears that a high proportion of the molybdenum ions is also present at another oxidation state. We assume that this oxidation state is equal to +IV. The lack, in all our spectra, of the two resonances evidenced in the reference MoO_2 shows that molybdenum did not form inclusions of this oxide in the matrix.

4. Discussion

Depending on the depth analyzed, the chemical state of molybdenum is completely different. Thus, in the first atomic layers detected, molybdenum is present as a Mo_4O_{11} intermediate oxide type. Indeed, as described in Section 3.4.1, even if many phases of the U–Mo–O diagram were evidenced [30,33,34], none was identified in nuclear fuel, and this whatever the burn-up. A reaction of UO_2 with the molybdenum present at the grain surface then seems very unlikely. Thus, the most probable situation seems to be the presence of an intermediate molybdenum oxide at both surface and grain boundaries. Indeed, whatever the annealing time, the same two components, located at 2528.8 and 2526.0 eV, are always present. Only their relative intensities vary depending on the annealing, indicating that the local environment of molybdenum ions present in UO_2 grains is described by the peaks located at 2523.9 eV and 2526.0 eV. This observation is confirmed by the fact that these components are systematically observed in the fluorescence measurements.

In our experimental spectra, the presence of these two peaks was attributed to the presence of Mo^{+IV} ions. However, because these are close to the edge of metallic molybdenum, the conclusion was that these components were convoluted, for the first, with the response of metallic Mo and, for the second, with that of a Mo^{+VI} oxide. For this oxidation state (+IV), a 2.0 eV gap is measured between the two energy levels of the 4d orbitals. This low value indicates that molybdenum does not have an octahedral symmetry. Indeed, in this case, as observed for MoO_2, a 2.6 eV gap was expected.

According to the crystal field theory [35], it is known that, for a metallic cation, the difference between the energy levels of the 4d orbitals in an octahedral symmetry is systematically higher than that of a cubic and even more so, for a tetrahedral ($\Delta E_{\text{tetra}} = 1/2 \times \Delta E_{\text{cubic}}$) symmetry. Moreover, as shown by our measurements at the oxygen K edge, the UO_2 matrix, even if it has an oxygen hyper-stoichiometry, keeps its cubic face-centred structure. In this structure, each uranium is surrounded by a cube made of eight oxygen atoms at 2.368 Å. Thus, the crystal field around the U^{+IV} ions has a cubic symmetry. Moreover, in the fluorite structure, one cationic site out of 2 is occupied by uranium, the other being vacant.

As no reference compounds with this Mo local symmetry could be available, we make ab initio calculation in order to simulate the spectra. We used the FDMNES code developed by Joly [36]. This code is based on the finite difference method and is not constrained to the muffin-tin approximation. Using this formalism, FDMNES can calculate XANES spectra at low energy and gives excellent results [37,38]. We used as input data, the crystallographic positions of the UO_2 cell with a molybdenum atom at $(0, 0, 0)$. This configuration is representative both of the Mo/U substitution and Mo in cationic vacancy. In these two cases, the local environments are the same, thus we will not be able to discriminate one of the two possibility. We made calculations with the cluster radius varying up to 5 Å in order to incorporate the first uranium shell (3.87 Å) and the next oxygen one (4.54 Å). As expected, no impact on white line is observed.

In Fig. 12, we reported the convoluted and unconvoluted calculated XANES spectra in full line and the fluorescence spectrum of the 48 h annealed sample. Except at the end of the experimental spectra (third component at 2528.4 eV) theory appears to be in good agreement with experiment.

In the theoretical spectra, we can clearly see the two components corresponding to 4d orbital splitting due to the cubic crystal field around Mo atoms. The energy gap obtained is 1.8 eV which is very close to the experimental

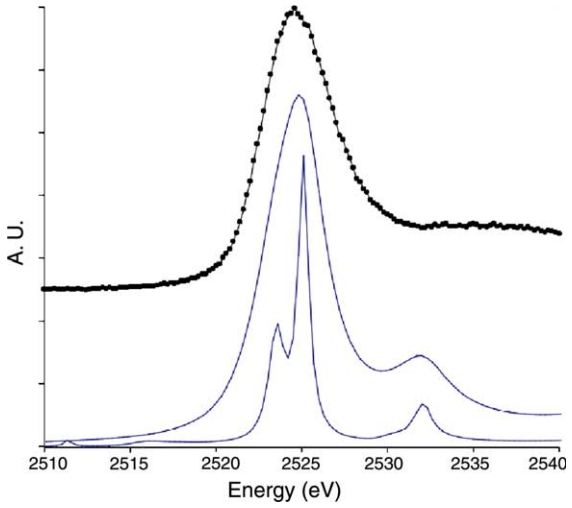

Fig. 12. XANES spectra obtained for the 48 h annealing samples measured in fluorescence (—●—) compared with FDMNES results before and after convolution (—).

one measured in annealed samples (2.0 eV). The absence of third component in the calculated spectrum confirmed that this one, as proposed, corresponds to another Mo environment.

According to this result, it can be assumed that the Mo ions in solution in the UO_2 matrix have a cubic symmetry and are therefore in the cationic position of the fluorite structure.

The weak oxidation of the sample surface during their transportation evidenced here, can be used to draw a parallel with reactor operations. Thus, as described in the introduction, molybdenum would act as a buffer, absorbing a fraction of the oxygen released by uranium fission. The fact that, in all our samples, molybdenum was detected at the oxidation state +IV would probably mean that a fraction of the excess oxygen present during implantation would be bound to this element without precipitating as MoO_2. The distribution of intragranular molybdenum between metallic and Mo^{+IV} states, evidenced in our measurements, would thus be the direct consequence of the initial hyper-stoichiometry, which would explain, on the one hand, its very weak evolution during reducing annealings and on the other hand, that its solubility is definitely more significant than that measured by Kleykamp [6].

By computing simulation, Nicoll et al. [4] highlighted that in stoichiometric $UO_{2.00}$, molybdenum would be present in a metallic state or in a standard Schottky defect. But as soon as an hyper-stoichiometry is present, molybdenum would be oxidised, in accordance with the results of thermochemistry and would be positioned in a cationic site. These simulations seem to confirm our experimental observations.

As proposed in the introduction, from the very beginning of reactor operation, a fraction of molybdenum is oxidised in Mo^{+IV}, while remaining in solution in the matrix, thus playing the role of buffer in the oxidation of UO_2.

5. Conclusion

In this work, X-ray absorption spectroscopy is proven to be a powerful tool to study nuclear fuel and fission products. By combining the measurements at the oxygen K and molybdenum L_{III} edges, we evidenced a correlation between the chemical form of molybdenum and the oxidation state of the UO_2 matrix. Our results, similar to those obtained on irradiated fuel, validate the use of ionic implantation on fresh UO_2 to simulate irradiated fuel. According to the results described herein, the behaviour of molybdenum in UO_2 can be summarised in three points:

- At the grain surface and boundaries, molybdenum, mainly in the Mo^{+VI} state, is present as an oxide, which would tend to disappear under reducing atmosphere. The precipitation of this phase is due to the fact that our samples are in contact with air between the thermal treatments and the XAS measurements. Accordingly, it is not representative of the evolution of molybdenum in reactor operation.
- Most of the remaining molybdenum is located in the grains of the matrix and appears to be divided between the oxidation states +IV and 0. The presence of Mo^{+IV} is due to the existence of an oxygen hyper-stoichiometry, confirming the buffer role of molybdenum in nuclear fuel. Moreover, these ions do not form MoO_2 inclusions and are inserted in the cationic positions of the crystal lattice of UO_2.
- Despite the absence of the other noble metals, such as Tc, Ru, Rh and Pd, molybdenum is present in its metallic form.

To our knowledge, this study is the first experimental evidence of the solution annealing of Mo^{+IV} in the cationic lattice of UO_2. Thus, when molybdenum is oxidised at the +IV state, it remains in solution in the UO_2 matrix. Its role in the solid swelling of nuclear fuel at low burn-up should be re-evaluated as described by Garcia et al. [7].

Acknowledgements

The authors thank A.M. Flank and P. Lagarde for their great help and technical support during the measurements performed on the LURE SA32 beamline, A. Plantier for the implantation at the IPN Lyon and F. Jollet for his contribution.

References

[1] H. Kleykamp, J. Nucl. Mater. 131 (1985) 221.
[2] R.W. Grimes, C.R.A. Catlow, Philos. Trans. R. Soc. London A 335 (1991) 609.
[3] S. Imoto, J. Nucl. Mater. 140 (1986) 19.
[4] S. Nicoll, H. Matzke, R.W. Grimes, C.R.A. Catlow, J. Nucl. Mater. 240 (1997) 185.
[5] S.G. Prussin, D.R. Olander, W.K. Lau, L. Hanson, J. Nucl. Mater. 154 (1988) 25.
[6] H. Kleykamp, J. Nucl. Mater. 206 (1993) 82.
[7] P. Garcia, J.P. Piron, D. Baron, in: Proceedings of Water Reactor Fuel Element Modelling at High Burnup and its Experimental Support, IAEA-TECDOC-957, 1997, p. 523.
[8] P. Martin, M. Ripert, T. Petit, T. Reich, C. Hennig, F. D'Acapito, J.L. Hazemann, O. Proux, J. Nucl. Mater. 312 (2003) 103.
[9] D.J. Jones, J. Roziere, G.C. Allen, P.A. Tempest, J. Chem. Phys. 84 (1986) 6075.
[10] H. Aritani, T. Tanaka, T. Funabiki, S. Yoshida, K. Eda, N. Sotani, M. Kudo, S. Hasegawa, J. Phys. Chem. 100 (1996) 19495.
[11] F.J. Ziegler, U. Littmark, J.P. Biersack, The Stopping and Range of Ions in Solids, Pergamon, New York, 1996.
[12] J. Purans, A. Kuzmin, P. Parent, C. Laffon, Electrochim. Acta 46 (2001) 1973.
[13] F. Jollet, T. Petit, N. Thromat, A. Pasturel, M. Gautier-Soyer, J. Phys.: Condens. Matter 9 (1997) 9393.
[14] Z.Y. Wu, F. Jollet, S. Gota, N. Thromat, M. Gautier-Soyer, T. Petit, J. Phys:. Condens. Matter 11 (1999) 7185.
[15] M. Pedio, J.C. Fuggle, J. Somers, E. Umbach, J. Haase, T. Lindner, U. Hofer, M. Grioni, F.M.F. De Groot, B. Hillert, L. Becker, A. Robinson, Phys. Rev. B 40 (1989) 7924.
[16] D.C. Koningsberger, R. Prins, X-Ray Absorption: Principles, Applications, Techniques of EXAFS, SEXAFS and XANES, Wiley-Interscience Publication/John Wiley, New York/Chichester/Brisbane/Toronto/Singapore, 1988.
[17] G.C. Allen, N.R. Holmes, J. Nucl. Mater. 223 (1995) 231.
[18] A.D. Murray, B.T.M. Willis, J. Solid State Chem. 84 (1990) 52.
[19] B.T.M. Willis, J. Phys. 25 (1964) 431.
[20] B.T.M. Willis, Acta Crystallogr. A 34 (1978) 88.
[21] G.C. Allen, P.A. Tempest, J.W. Tyler, Nature 295 (1982) 48.
[22] L. Nowicki, F. Garrido, A. Turos, L. Thome, J. Phys. Chem. Solids 61 (2000) 1789.
[23] L. Kihlborg, Ark. Kemi 21 (1963) 357.
[24] R.W.G. Wyckoff, Crystal Structure, Interscience, 1963.
[25] H. Aritani, T. Tanaka, T. Funabiki, S. Yoshida, M. Kudo, S. Hasegawa, J. Phys. Chem. 100 (1996) 5440.
[26] S.R. Bare, G.E. Mitchell, J.J. Maj, G.E. Vrieland, J.L. Gland, J. Phys. Chem. 97 (1993) 6048.
[27] T. Ressler, R.E. Jentoft, J. Wienold, M.M. Gunter, O. Timpe, J. Phys. Chem. B 104 (2000) 6360.
[28] A. Magneli, Acta Crystallogr. 6 (1953) 495.
[29] O.G. D'yachenko, V.V. Tabachenko, R. Tali, L.M. Kovba, B.O. Marinder, M. Sundberg, Acta Crystallogr. B 52 (1996) 961.
[30] V.V. Tabachenko, O.G. D'yachenko, Eur. J. Solid State Inorg. Chem. 32 (1995) 1137.
[31] C. Gaillard, N. Chevarier, C. Den Auwer, N. Millard-Pinard, P. Delichere, P. Sainsot, J. Nucl. Mater. 299 (2001) 43.
[32] S.R. Bare, Langmuir 14 (1998) 1500.
[33] N.L. Misra, K.L. Chawla, V. Venupogel, N.C. Jayadevan, D.D. Sood, J. Nucl. Mater. 226 (1995) 120.
[34] M. Ugajin, T. Nagasaki, A. Ttoh, J. Nucl. Mater. 230 (1996) 195.
[35] E. Huheey, E.A. Keiter, R.L. Keiter, Inorganic Chemistry: Principles of Structure and Reactivity, Boeck & Larcier s.a., Paris, 1996.
[36] Y. Joly, Phys. Rev. B 63 (1996) 125120.
[37] Y. Joly, J. Synch. Radiat. 10 (2003) 58.
[38] S. Di Matteo, T. Chatterji, Y. Joly, A. Stunault, J.A. Paixao, R. Suryanarayanan, G. Dhalenne, A. Revcolevschi, Phys. Rev. B 68 (2003) 24414.